HHS Public Access

Author manuscript

Nat Cell Biol. Author manuscript; available in PMC 2015 April 01.

Published in final edited form as:

Nat Cell Biol. 2014 October ; 16(10): 1004–13. doi:10.1038/ncb3040.

ΔNp63 promotes stem cell activity in mammary gland development and basal-like breast cancer by enhancing Fzd7 expression and Wnt signaling

Rumela Chakrabarti[1], **Yong Wei**[1], **Julie Hwang**[1], **Xiang Hang**[1], **Mario Andres Blanco**[1,2], **Abrar Choudhury**[1], **Benjamin Tiede**[1], **Rose-Anne Romano**[3], **Christina DeCoste**[1], **Laura Mercatali**[4], **Toni Ibrahim**[4], **Dino Amadori**[4], **Nagarajan Kannan**[5], **Connie J Eaves**[5], **Satrajit Sinha**[3], and **Yibin Kang**[1,6]

[1]Department of Molecular Biology, Princeton University, Princeton, NJ 08544

[2]Boston Children's Hospital, Harvard Medical School, Boston, MA 02115

[3]Department of Biochemistry, Center of Excellence in Bioinformatics and Life Sciences, State University of New York at Buffalo, Buffalo, NY 14203

[4]Osteoncology and Rare Tumors Center, Istituto Scientifico Romagnolo per lo Studio e la Cura dei Tumori (IRST), IRCCS, Meldola, Italy

[5]Terry Fox Laboratory, British Columbia Cancer Agency, Vancouver, British Columbia V5Z 1L3, Canada

[6]Rutgers Cancer Institute of New Jersey, New Brunswick, NJ 08903

Abstract

Emerging evidence suggests that cancer is populated and maintained by tumor initiating cells (TICs) with stem-like properties similar to that of adult tissue stem cells. Despite recent advances, the molecular regulatory mechanisms that may be shared between normal and malignant stem cells remain poorly understood. Here we show that the ΔNp63 isoform of the Trp63 transcription factor promotes normal mammary stem cell (MaSC) activity by increasing the expression of the Wnt receptor Fzd7, thereby enhancing Wnt signaling. Importantly, Fzd7-dependent enhancement of Wnt signaling by ΔNp63 also governs tumor initiating activity of the basal subtype of breast

Communications to: Yibin Kang, Department of Molecular Biology, LTL 255, Princeton University, Princeton, NJ 08544, Phone: 609-258-8834, Fax: 609-258-2340, ykang@princeton.edu.

AUTHOR CONTRIBUTIONS

R.C. and Y.K. designed experiments. R.C., Y.W., J.H., X. H., M.A.B., A.C, B.T., N.K. and S.S. performed the experiments. T. I., L. M., D.A., R.R., C.D., N. K. and C.J.E. provided crucial samples and technical advice. R.C. and Y.K. wrote the manuscript. All authors discussed the results and commented on the manuscript.

COMPETING FINANCIAL INTERESTS

The authors declare no competing financial interests.

Accsssion numbers for datasets

Microarray data generated in this study have been deposited at the NCBI Gene Expression Omnibus (http://www.ncbi.nih.gov/geo/) with the accession code GSE47493. Other published datasets used in this study are GSE22446 (MaSC signature)[64] and GSE2034 (EMC286 dataset)[47]. The processed TCGA RNAseq data is obtained from UCLA Cancer Browser https://genome-cancer.ucsc.edu/proj/site/hgHeatmap/. Dataset ID: TCGA_BRCA_exp_HiSeqV2_exon, version 2013-12-18.

cancer. These findings establish ΔNp63 as a key regulator of stem cells in both normal and malignant mammary tissues and provide direct evidence that breast cancer TICs and normal MaSCs share common regulatory mechanisms.

The mechanisms and pathways regulating self-renewal and differentiation of MaSCs are of great interest for its potential application in prevention and treatment of breast cancer[1]. TICs, also known as cancer stem cells (CSCs), play key roles in treatment resistance, recurrence, and metastasis of breast cancer and other malignant diseases[2–4], and may share similar features and regulatory mechanisms with normal stem cells. However, despite significant progress in recent years, the molecular basis underlying the putative link between TICs and normal tissue stem cells remains poorly characterized.

Recent studies have highlighted several transcription factors (TFs), such as Bmi-1, Oct1, p53, Snail, Gata3 and Elf5, as key regulators with multiple roles in mammary cell fate determination, stem cell activity, tumor initiation and progression[5–10]. Transformation-related protein 63 (Trp63, or p63) is a member of the p53/p63/p73 family TFs that is highly expressed in stratified epithelia such as cervix, skin, prostate and breast[11]. p63 proteins include isoforms of two major groups: those possessing a full-length transactivation domain (referred to as the TA isoforms), and those lacking this domain (the ΔN isoforms)[11, 12]. The role of p63 in development and cancer has remained perplexing largely because of these multiple isoforms of p63. Both increased and reduced expression of p63 have been observed in human cancers[13, 14]. Disparate results regarding the role of p63 in cancer have also been reported using different p63 mouse models[15, 16]. It has been suggested that the TA isoforms are most similar to p53 in their tumor suppressive functions[17,18] and the ΔNp63 isoforms generally exhibit oncogenic functions, such as in skin and bladder[19, 20]. In the normal mammary gland, ΔNp63 is shown to be expressed at much higher levels than TAp63[21–24]. Recent studies have also revealed a role of ΔNp63 in maintaining basal lineage cell fate *in vitro* in mammary epithelia cells[25]. Despite these findings, rigorous functional studies of p63 isoforms in regulating MaSCs and TICs remain scarce and warrant further investigation.

The role of p63 in regulating epithelial homeostasis has been linked to its influence on several signaling pathways such as Notch, Wnt, and Shh[26–29], which have all been shown to be important regulators of normal and cancerous stem cells[30, 31]. The extent to which these pathways are involved in p63-dependent regulation of mammary epithelium remains unclear. Notably, Wnt signaling has been shown to be instrumental for mammary gland development and MaSC activity[32–34]. Aberrant Wnt signaling has also been reported in tumors from patients with different types of cancers such as colorectal cancer, hepatocellular carcinoma, hepatoblastoma, and breast cancer[35–37]. In breast cancer, Wnt signaling has been found to be particularly hyperactive in the basal-like subtype and predicts poor prognosis[38, 39]. However, what regulates Wnt signaling in normal MaSCs and the highly aggressive basal subtype of breast cancer remains poorly understood. In general, oncogenic mutations in Wnt pathway components, such as β-catenin, APC and Axin, are relatively rare in breast cancer[40, 41].

In this study, we dissect the role of different p63 isoforms in MaSCs and breast cancer TICs. Using multiple isoform-specific molecular and genetic tools and models, we demonstrate the

important function of ΔNp63 in regulating MaSC activity and promoting breast cancer initiation in basal-like breast cancer *via* direct transcriptional activation of *Fzd7* and subsequent enhancement of Wnt signaling.

RESULTS

ΔNp63 but not TAp63 regulates MaSC activity

To identify candidate regulators of MaSCs, we performed transcriptomic analyses of different mammary epithelial cell (MEC) subpopulations isolated by FACS from the mouse mammary epithelium, including $Lin^{-}CD24^{+}CD29^{hi}$ (P4, representing MaSC-enriched basal populations) and $Lin^{-}CD24^{+}CD29^{lo}$ (P5, representing luminal cells). Global transcriptome analyses revealed 26 transcriptional regulators that have >3 fold higher expression in P4 versus P5 populations (Fig. 1a, upper panel, and Supplementary Table 1). Among these, *p63* expression is most strongly elevated by more than 45 folds in the P4 population. Isoform-specific mRNA and protein analyses confirmed that ΔNp63, but not TAp63, is the primary p63 isoform expressed in primary MECs and MaSC-enriched MECs in both mouse and human (Fig. 1a–d and Supplementary Fig. 1a).

To explore the functional importance of ΔNp63 in MaSCs, ΔNp63 and TAp63 expressing lentiviral vectors were transduced into MECs (Fig. 1e and Supplementary Fig. 1b,c), and robust ectopic overexpression of both genes was confirmed (Supplementary Fig. 1d,e). Interestingly, overexpression of ΔNp63, but not TAp63, in P4 cells led to a significant increase in MaSC activity, as reflected by increased reconstitution and ductal outgrowth after transplantation into cleared fat pad (Fig. 1f and Supplementary Fig. 1f,g). Importantly, ΔNp63 overexpression also conferred stem cell activity to P5 cells, indicating that ΔNp63 is able to induce luminal cells to enter a stem-like state (Fig. 1g and Supplementary Fig. 1h,i). We next measured ΔNp63-induced enhancement of MaSC activity using a more stringent competitive reconstitution assay[8, 34] (Supplementary Fig. 1j). Transplantation of ΔNp63-$dsRED^{+}$ and control-GFP^{+} P4 cells in equal ratio resulted in outgrowths that were predominantly $dsRED^{+}$, suggesting that ΔNp63-overexpressing MaSCs had competitive growth advantage over their normal counterparts (Fig. 1h,i). In contrast, overexpression of TAp63 did not augment MaSC ability (Fig. 1h,i). Collectively, these studies demonstrate that ΔNp63, but not TAp63 promotes MaSC activity.

We next examined the function of ΔNp63 in different subpopulation of luminal cells. CD61 has been described to be a luminal progenitor marker among luminal epithelial cells (P5)[42]. Overexpression of ΔNp63 increased the repopulating frequency in both P5-$CD61^{+}$ and P5-$CD61^{-}$ population (Supplementary Fig. 2a,b). Additionally, immunostaining of 3-D matrigel colonies and mammary outgrowths from ΔNp63 overexpressing $CD61^{+}$ and $CD61^{-}$ luminal subsets with cytokeratin 14 and 8 (K14 and K8) markers revealed cells from both basal and luminal lineages, suggesting the capability to differentiate into both lineages (Supplementary Fig. 2c,d). Interestingly, ΔNp63 overexpression failed to significantly increase reconstitution in $Lin^{-}CD24^{lo}$ (P6) stromal-enriched cells (Supplementary Fig. 2e,f), suggesting that its function is restricted to epithelial cells.

ΔNp63-overexpressing outgrowths showed increased tertiary branching and increased percentage of Ki67 positive cells (Fig. 1f and Supplementary Fig. 3a,b), suggesting that increased proliferation may in part account for the enhanced branching associated with ΔNp63 overexpression. An increased presence of ΔNp63 and K14 positive basal cells (Supplementary Fig. 3c–e) is consistent with FACS analysis of outgrowths showing a ~2-fold increase of P4 population in the ΔNp63-overexpressing mammary epithelium (Supplementary Fig. 3f,g).

We next investigated the effect of ΔNp63 and TAp63 overexpression on colony-forming abilities. A significant increase in clonogenic potential was observed in MaSCs overexpressing ΔNp63 compared to TAp63 in primary 3-D matrigel cultures (Supplementary Fig. 4a,b). Monochromatic colonies formed by mixed P4 cells from Actin-GFP and Actin-DsRed mammary glands confirmed that each colony originates from single cells instead of aggregates (Fig. 1j). We next performed serial passage and transplantation assays both *in vitro* and *in vivo,* which confirmed that ΔNp63 can induce MaSC self-renewal activity (Fig. 1k,l and Supplementary Fig. 4c).

To further test whether the observed ΔNp63 phenotype is dependent on its transcriptional activity, we tested a DNA binding mutant (MT) form of ΔNp63 in P4 cells. While similar levels of MT and wild type (WT) ΔNp63 were overexpressed in these cells (Supplementary Fig. 4d,e), only WT ΔNp63 induced the increased MaSC activity as shown by the matrigel colony formation and reconstitution assays (Supplementary Fig. 4f–h).

Loss of ΔNp63 leads to MaSC deficiency

To complement our gain-of-function analysis of ΔNp63 as described above, we next used a ΔNp63-GFP knock-in loss-of-function mouse model (Supplementary Fig. 5a)[43]. Since homozygous loss of ΔNp63 leads to embryonic lethality, we performed all of our experiments using heterozygous $\Delta Np63^{gfp/+}$ animals with reduced expression of ΔNp63 (Fig. 2a,b). We observed a significant reduction of ductal elongation in $\Delta Np63^{gfp/+}$ mammary glands compared to those of WT counterparts at both 6 weeks and 9–10 weeks (Fig. 2c and Supplementary Fig. 5b–d). FACS and limiting dilution assays also demonstrated reduced number and activity of MaSCs in $\Delta Np63^{gfp/+}$ mice (Fig. 2d–f, and Supplementary Fig. 5b,d,e).

To further evaluate the loss-of-function effect of individual p63 isoforms, we next performed isoform-specific knockdown (KD) of ΔNp63 and TAp63 in mouse MECs (Fig. 2g–i). As expected, only ΔNp63 KD led to significantly reduced mammosphere numbers, suggesting decreased stem cell activity (Fig. 2j). Together, these results indicate that ΔNp63 but not TAp63 is a crucial regulator of normal MaSCs.

To obtain a global view of the molecular events underlying the loss of ΔNp63 phenotype, we next performed a microarray analysis of control and $\Delta Np63^{gfp/+}$ MECs (Fig. 2k). Gene-set enrichment analysis (GSEA) demonstrated that MaSC-enriched genes were significantly down-regulated in the transcriptome of $\Delta Np63^{gfp/+}$ MECs (Fig. 2k), a finding consistent with the decreased MaSC activity of $\Delta Np63^{gfp/+}$ MECs.

Wnt receptor Fzd7 is a ΔNp63 target that mediates its effect on MaSCs

Multiple lines of evidence suggest that Notch, Wnt and Shh signaling is important for stem cell activity in different tissues[31]. Therefore, we next investigated if any of these pathways were altered in ΔNp63$^{gfp/+}$ MECs. GSEA demonstrated that only Wnt signaling gene sets were significantly down-regulated in both MECs and P4 cells from ΔNp63$^{gfp/+}$ mice compared to WT (Fig. 3a). To directly test whether ΔNp63-regulated Wnt signaling is important for MaSC function, we performed colony formation assays with and without Wnt signaling inhibitor Dickkoph 1 (Dkk1). Dkk1 inhibited ΔNp63-mediated increase in colony formation of both primary cells and cells in subsequent serial passages (Supplementary Fig. 5f–h), suggesting that ΔNp63-induced MaSC activity is indeed mediated by Wnt signaling. Moreover, Wnt reporter assay confirmed positive regulation of canonical Wnt signaling in MaSCs by ΔNp63 but not TAp63 (Fig. 3b).

We next sought to identify Wnt signaling genes regulated by ΔNp63. Transcriptome profiling indicated that nine Wnt pathway genes, including several Wnt ligands and receptors, have reduced expression in ΔNp63$^{gfp/+}$ P4 cells compared to WT (Fig. 3c). qRT-PCR analysis confirmed four out of these nine genes to be significantly down-regulated in ΔNp63$^{gfp/+}$ MaSCs (Fig. 3d). Among these, only one receptor and one ligand gene, *Fzd7* and *Wnt5a*, have reduced expression after acute lentivirus-mediated KD of p63 in primary MECs (Fig. 3e). Notably, both *Wnt5a* and *Fzd7* belonged to the "enrichment cores" of two WNT gene signatures used in the GSEA study (Supplementary Fig. 6a). Therefore, we hypothesized that ΔNp63 may regulate MaSCs *via* direct activation of either *Fzd7* or *Wnt5a,* or both. To further investigate this possibility, we next performed isoform-specific KD of p63. Reduced levels of *Fzd7* and not *Wnt5a* were observed with ΔNp63 KDs but not TAp63 KDs (Fig. 3f,g). Conversely, enforced overexpression of ΔNp63 but not TAp63 led to a significant increase in expression of both *WNT5A* and *FZD7* in the HMLE human mammary epithelial line (Fig. 3h, right panel, and Supplementary Fig. 6b). Interestingly, only *FZD7* showed strong activation by ΔNp63 within 48 hours post-infection, suggesting it to be a direct target of ΔNp63 (Fig. 3h, left panel). Indeed, examination of ChIP-seq data of human keratinocytes[44] revealed p63 binding in a conserved active enhancer region ~40Kb upstream from *FZD7* gene (Fig. 3i, region highlighted in red). To confirm binding of p63 to this enhancer, we performed ChIP analysis of primary human MECs (HMEC) and primary mouse MMTV-Wnt1 tumor cells using anti-p63 antibodies, and observed strong enrichment of the *FZD7* enhancer in p63-bound chromatin (Fig. 3j,k). We next performed luciferase assays using a reporter driven by the *FZD7* enhancer, together with ΔNp63, TAp63, or a DNA-binding mutant of ΔNp63. As expected, only ΔNp63 overexpression significantly activated *FZD7* enhancer reporter activity in HMLE cells and immortalized murine mammary epithelial cells (iMMECs)[45] (Fig. 3l,m).

We next determined the direct functional importance of Fzd7 in MaSCs. Fzd7 overexpression in P4 cells led to increased MaSC activities, phenocopying the effect of ΔNp63 (Fig. 4a,b). Moreover, overexpression of Fzd7 in ΔNp63$^{gfp/+}$ P4 cells was able to at least partially rescue the reduced MaSC phenotype close to that of the wild type levels in both colony formation (Fig. 4c,d) and repopulation assays (Fig. 4e,f). Similarly, Fzd7 overexpression rescued MaSCs activity in ΔNp63-KD MECs (Supplementary Fig. 6c,d).

Finally, Fzd7 KD attenuated the increase in MaSC activity driven by ΔNp63 overexpression (Fig. 4g,h). Collectively, these data suggest that ΔNp63-induced MaSC activity is primarily mediated by increasing the expression of Wnt signaling receptor Fzd7.

Positive correlation of ΔNp63 and Fzd7 expression in human tumors

To evaluate the relationship between ΔNp63 and overall WNT signaling activity in the clinical setting, we interrogated two human breast cancer datasets[46, 47]. Consistent with the $\Delta Np63^{gfp/+}$ mouse data (Fig. 3a), GSEA of the EMC286 dataset revealed a significant enrichment of WNT signaling gene sets in human breast tumor samples predicted to have high ΔNp63 activity based on their ΔNp63-specific gene signature score (Supplementary Fig. 6e). High ΔNp63 signature expression is preferentially associated with the basal subtype over the luminal subtype (Fig. 5a) and the ΔNp63 signature score showed a positive correlation with *FZD7* expression (Supplementary Fig. 6f). Further confirming this observation, analysis of a TCGA dataset containing isoform-specific RNA-Seq data[46] revealed Δ*Np63* as the primary *p63* isoform expressed in tumors (Supplementary Fig. 6g) and a strong positive correlation between Δ*Np63* and *FZD7* mRNA levels (Fig. 5b). Consistently, immunostaining of ΔNp63 and FZD7 in 12 primary human breast tumors revealed a similar positive correlation ($r = 0.47$, $p = 0.06$) based on staining intensity score (Pearson correlation) (Fig. 5c), and both proteins were found to be upregulated in the triple-negative (TN) breast tumors compared to the luminal subtype ($p = 0.04$ and $p = 0.03$ for ΔNp63 and FZD7 respectively) (Fig. 5c). To further test the functional link between p63 and canonical Wnt signaling, we next performed Wnt reporter assays in the MDA-MB-231 breast cancer cell line. p63 KD led to a significant reduction of FZD7 protein level (Supplementary Fig. 7a), as well as inhibition of WNT3A-induced canonical Wnt signaling (Fig. 5d), to an extent comparable to FZD7 KD. As expected, p63 KD also led to reduced tumor engraftment of TN MDA-MB-231 and SUM-1315 cells (Supplementary Fig. 7b,c). Furthermore, KD of ΔNp63 but not TAp63 (Fig. 5e–h) led to significant inhibition of Wnt signaling (Fig. 5i), similar to pan-p63 KD using shRNAs targeting sequences encoding the DNA binding domain (DBD). Importantly, ΔNp63 but not TAp63 KD reduced tumor incidence to a degree similar to pan-p63 KD or FZD7 KD (Fig. 5j,k), and resulted in reduced FZD7 expression (Fig. 5f,g).

To further strengthen the molecular connection between ΔNp63 and FZD7 in human breast cancer, we next investigated the functional role of ΔNp63 and Fzd7 in three patient derived xenografts (PDX) of human TN breast tumors. Immunohistochemistry (IHC) on PDX tumors indicate strong expression of ΔNp63 and Fzd7 in all three PDX tumors compared to weak TAp63 staining in PDX-1 and PDX-3 tumors[48] (Supplementary Fig. 7d). Lentiviral KD of ΔNp63 and FZD7 in PDX tumors (PDX-2 and PDX-3) significantly reduced tumorsphere formation compared to control and TAp63 KD (Fig. 5l–p). Taken together, our data suggests that the ΔNp63-Fzd7-Wnt signaling axis is conserved in human breast cancer and regulates tumor formation.

ΔNp63 induces tumor initiating ability in basal-like mouse mammary tumors

To more rigorously test the functional role of ΔNp63 regulated Fzd7 expression in controlling TIC activity of basal-like breast cancer cells, we next performed IHC on tumors

derived from three different mouse models representing different subtypes of breast cancer based on gene expression profiling — MMTV-Wnt1 (basal), MMTV-Myc (mixed basal and luminal) and MMTV-PyMT (luminal)[49, 50]. As expected, higher expression of ΔNp63 and Fzd7 expression was observed in the basal subtype (MMTV-Wnt1) compared to luminal subtype (MMTV-PyMT) tumors (Supplementary Fig. 7e,f), further supporting observations from human breast cancers. Modest ΔNp63 staining and Fzd7 was also observed in MMTV-Myc tumors. In contrast, no positive TAp63 staining was observed in any tumor subtype (Supplementary Fig. 7e). Functionally, p63 KD in MMTV-Wnt1 tumor cells significantly reduced tumorsphere formation *in vitro* (Fig. 6a,b) and increased tumor latency and decreased tumor volume *in vivo* (Fig. 6c–e).

A small subset of $CD45^{-}CD24^{+}Thy\text{-}1^{+}$ cells in the MMTV-Wnt1 tumors is thought to be endowed with TIC properties[51]. We found that both p63-KD and Fzd7-KD tumor cells showed significant reduction of the $Thy\text{-}1^{+}$ population (Fig. 6f,g). Fzd7 expression was significantly decreased (Fig. 6h) after p63 KD, further suggesting *Fzd7* as a direct target of ΔNp63. Consistent with the isoform-specific role of ΔNp63 in regulating TIC activity, KD of ΔNp63 but not TAp63 reduced Fzd7 expression and tumorsphere formation (Fig. 6i–k).

We next directly investigated whether Fzd7 has any functional significance in Wnt1-driven tumor cells both *in vitro* and *in vivo*. Interestingly, Fzd7-KD in Wnt1 tumor cells decreased tumorsphere formation (Fig. 6l), phenocopying ΔNp63-KD. Furthermore, the reduced tumorsphere-forming activity of ΔNp63-KD Wnt1 tumor cells were rescued by ectopic expression of Fzd7 (Fig. 6l). Corroborating the *in vitro* data, Fzd7-KD cells showed increased tumor latency and significantly reduced tumor burden, phenocopying ΔNp63-KD (Fig. 6m–o). However, one potential caveat of using MMTV-Wnt1 tumor model to investigate the p63-Fzd7 regulatory axis is that Wnt1-induced tumors may depend on Fzd7 regardless of p63. To circumvent this problem, we performed p63 and Fzd7 KD in both MMTV-Myc and Blg-Cre-$Brca1^{f/f}$ $p53^{+/-}$ tumors that are not induced by Wnt. ΔNp63-KD in MMTV-Myc tumors yielded similar results to ΔNp63-KD in MMTV-Wnt1 tumors, such as decreased tumorsphere formation, increased tumor latency, and significantly reduced tumor burden (Fig. 7a–i). Furthermore, Fzd7 KD also led to reduced tumorsphere-forming ability of these two additional basal-like mouse mammary tumor models (Fig. 7j–k), suggesting a common role of Fzd7 in regulating basal-like tumors.

To more definitively examine the role of ΔNp63 in basal-like breast cancer, we generated MMTV-Wnt1; $\Delta Np63^{gfp/+}$ mice. Expression of *Wnt1* oncogene under the *MMTV* promoter led to extensive ductal hyperplasia and expansion of the MaSC-enriched basal (P4) population[32], a phenotype that is reduced in $\Delta Np63^{gfp/+}$ mice (Fig. 8a,b). Consistently, MMTV-Wnt1; $\Delta Np63^{gfp/+}$ MECs displayed reduced MaSC activity (Fig. 8c–e). Reduced expression of ΔNp63 in $\Delta Np63^{gfp/+}$ mice also led to significant delay in tumor initiation as well as reduction of Fzd7 and basal marker K14 expression (Fig. 8f and Supplementary Fig. 8a–c). These results indicate that ΔNp63 activity contributes to the regulation of the TIC population in Wnt1-induced pre-neoplasia and basal tumors.

DISCUSSION

p63 is a member of the p53 superfamily that is structurally similar but functionally distinct from p53[11]. The function of p63 has also been extended from regulating stem cells activity, differentiation, growth and survival to other aspects of cancer biology, such as cell adhesion[52] and metastasis[13]. Despite these advances, the functional role of p63 in regulating MaSCs remains unclear. Overexpression of ΔNp63 in unsorted MECs *in vitro* was found to result in an increase in basal cells but reduced regenerative potential by antagonizing Notch[25]. In our current study, we used isoform-specific lentiviral overexpression in primary MaSCs to show that ΔNp63 overexpression promotes MaSC activity while genetic ablation of even one allele of Δ*Np63* reduces MaSC function *in vivo*. We also demonstrated that the ΔNp63 isoform regulates these phenotypes through upregulating Wnt signaling while the TAp63 isoform does not have such effects, highlighting the importance of isoform-specific studies of p63 gene in development and cancer. Furthermore, ΔNp63 overexpression can convert luminal cells to a stem-like state, supporting the emerging concept of reversible plasticity in epithelial cell fate[3, 4, 8, 25, 53].

The role of ΔNp63 in breast cancer remained largely unclear despite some recent exploration of p63 functionality in breast cancer initiation[54]. We establish a functional role of ΔNp63 in regulating TICs in basal breast cancer, an aggressive form of breast cancer with few available treatment options[55–57]. ΔNp63-specific gene signature is highly enriched in this subtype and ΔNp63-specific KD severely diminishes TIC activity of basal breast cancer cells. Taken together, our studies establish ΔNp63 as a functional driver of normal and malignant stem cells in the mammary epithelium (Fig. 8g).

FZD7 is one of the most abundant Frizzled family proteins expressed in basal/TN breast cancer, and has been shown to promote proliferation of these tumors[38, 58, 59]. However, the role of Fzd7 in mammary gland development and the mechanism of its elevated expression in basal/TN breast cancer remain poorly defined. We identified Fzd7 as a direct transcriptional target of ΔNp63 and demonstrated that Fzd7 functions downstream of ΔNp63 in regulating MaSC activity. Despite the strong correlation of Fzd7 and ΔNp63 expression in clinical samples, we do not rule out the possibility that Fzd7 expression could be regulated by additional mechanisms. Our findings thus establish a paradigm for Wnt pathway activation in basal-like breast cancer that do not depend on oncogenic mutation of Wnt pathway components, as commonly seen in colorectal cancer, heptocellular carcinoma and other cancers[36, 40, 41, 60]. The ΔNp63-FZD7-Wnt axis may represent a driving force for the initiation and maintenance of basal-like breast tumor, thus serving as a potential target for therapeutic intervention.

The cell of origin of TICs in different subtypes of breast cancer remains ill-defined despite some recent advances. Gene expression profiling and targeted disruption of *BRCA1* in mouse models suggest that luminal progenitors are likely target cell population of basal-like breast cancer harboring *BRCA1* mutations[1, 61, 62]. In our current study, heterozygous loss of ΔNp63 reduces expansion of the MaSC-enriched P4 population in the pre-neoplastic mammary gland hyperplasia, as well as reduction of the Thy-1$^+$ TIC population in MMTV-Wnt1 tumors. These findings suggest that MaSCs may be the cell of origin in another subset

of basal-like breast cancers that is dependent on the ΔNp63-Fzd7-Wnt axis. Given the heterogeneity of basal-like breast cancers, it is not surprising that under the influence of different oncogenic events, distinct target cell population in the normal gland may give rise to TICs in different subsets of basal-like breast cancer. It is also possible that during oncogenic transformation of luminal progenitors, MaSC-like features as well as elevated ΔNp63 expression might be acquired in TICs or their pre-neoplastic precursors that eventually give rise to basal-like cancers (Fig. 8g). Future studies are required to rigorously explore these various possibilities.

METHODS

Animal studies

Animal procedures were conducted in compliance with Institutional Animal Care and Use Committee (IACUC) of Princeton University. ΔNp63-GFP knock-in mouse model has been described previously[43]. For all experiments, $\Delta Np63^{gfp/+}$ (ΔNp63-heterozygote) and control littermate (WT) animals were utilized. MMTV-Wnt1 (C57/B6 background) animals were crossed to $\Delta Np63^{gfp/+}$ mice (C57/B6 background) to give rise to MMTV-Wnt1; $\Delta Np63^{+/+}$ and MMTV-Wnt1; $\Delta Np63^{gfp/+}$ females. For cleared fat pad injection experiment, FVB or C57/B6 mice at 3 weeks old were anaesthetized and a small incision was made to reveal the mammary gland. Single cell injections involved sorted mammary epithelial cells into cleared inguinal (#4) mammary fat pads according to standard injection procedures[32]. For orthotopic primary tumor formation, FVB mice were used, since MMTV-Wnt1 or MMTV-cMyc animals for this experiment were on FVB background. MMTV-Wnt1 or MMTV-cMyc tumor cells resuspended in 10 μl PBS: matrigel (1:1) were injected directly into the mammary fat pad. MDA-MB-231 or SUM-1315 cells resuspended in 10 μl PBS: matrigel (1:1) were injected in mammary fat pad of immunocompromised NSG mice. The primary tumor growth was monitored weekly. We used 6–10 mice per experimental group in all animal experiments. All animals were of the same age and sex at the time of mammary epithelial cell injection or tumor cell injection. No statistical method was used to pre-determine sample size. The experiments were not randomized. There was no blinded allocation during experiments and outcome assessment. However, the technicians who performed the measurement of tumor size or repopulation percentage and area were blind to the allocation.

Limiting dilution assay (LDA)

Single cell suspension of primary MECs from WT and $\Delta Np63^{gfp/+}$ mammary glands at 6–7 or 9–10 weeks were sorted in combination with the Lin^-, $CD24^+$, and $CD29^{hi}$ markers to obtain MaSC-enriched P4 ($Lin^-CD24^+CD29^{hi}$) cells, which were then injected into cleared mammary fat pads. The outgrowths were analyzed at 6–8 weeks post-transplantation. Transplantation was performed with indicated number of cells resuspended in 50% Matrigel and 50% PBS. Frequency of MaSCs in transplanted cell suspension was calculated using L-calc software (StemCell Technologies) or ELDA (Extreme Limiting Dilution Assay)[50]. Single hit model was also tested using ELDA and value of slope was 1. MaSC abundances were assumed to follow a Poisson distribution in LDAs, and generalized linear models utilizing a log-log link function were used to derive repopulation frequency parameters. For

human MaSCs enriched population, we FACS purified basal cell population from healthy breast tissues obtained from reduction mammoplasties using previously described approaches[65]. For competitive reconstitution assay, 2000 MaSC-enriched populations (P4) isolated from Actin-GFP and Actin-DsRed mice were mixed in equal ration (1:1) either from control or experimentally manipulated cells and injected into cleared mammary fat pad.

Mammosphere/tumorsphere and 3D matrigel colony forming assays

Stem cells from the mammary gland have been maintained and passaged *in vitro* as spheroids in suspension or as organoids in 3-D matrigel cultures. Mammosphere counts from either method over multiple passages represent self-renewal activity[8]. Cells were cultured as previously described[10]. Briefly, primary mammary epithelial cells from normal gland or tumor tissue were spin infected and then plated either onto six-well, ultra-low attachment plates (Corning) at a density of 10,000 cells/ml or 20,000 cells/ml for mammosphere or tumorsphere assay. For 3-D colony forming assay, cells were plated in reduced growth factor matrigel (BD Biosciences) at a density of 10,000 or 20,000 cells.

Cell lines and culture conditions

HMLE cells were cultured in DMEM/F12 (1:1) media containing 5% horse serum, 10μg/ml insulin, 20 ng/nl EGF, 100ng/ml cholera toxin and 500ng/ml Hydrocortizone. iMMEC cells were cultured in F12 media containing 10% fetal bovine serum, 10μg/ml insulin, 20 ng/nl EGF and 500ng/ml Hydrocortizone. HMEC cells (Lonza) were cultured in media in accordance with manufacturer's instructions.

Molecular cloning

The pLEX plasmids (Open Biosystems) containing cDNAs for control-GFP, WT-ΔNp63, MT-ΔNp63 and WT-Fzd7 were generated by routine molecular cloning techniques. The WT-ΔNp63 and MT-ΔNp63 cDNAs were subcloned from pCMV-HA vector, to pLEX plasmids using BamHI-XhoI/NotI restriction sites. *Fzd7* cDNA was subcloned to pLEX plasmids using BamHI-MluI restriction sites. The DNA-binding deficient MT-ΔNp63 represents an amino acid change R>W at position 304 and has been described before[43]. The 500 bp *Fzd7* enhancer segment was isolated from human genomic DNA by PCR and cloned into pGL3-basic (promega) using KpnI-SpeI restriction sites. For retroviral mediated knockdown studies, shRNAs targeting isoform-specific and/or common region of human and mouse p63 were designed using shRNA_selector as described[66]. The sense and antisense oligos of each shRNA were annealed and cloned into pRetroSuper vector using BglII and HindIII sites[67]. Empty vector was used as negative control. For lentivirus mediated isoform-specific shRNAs, the XhoI/NheI fragment containing H1 driven shRNA expression cassette were transferred from pRetroSuper vector to lentiviral vector pLEIGW so the resulting lentiviral vector expresses shRNA and EGFP as selection marker. For knockdown studies in mouse, *Fzd7* and *p63* (both isoforms) targeting shRNA expression lentiviral vectors were purchased from Sigma-Aldrich (St. Louis, MO, USA). The targeting shRNA sequences are: 5′-GAGGCCAACTCGCAGTACTTTC-3′ for *Fzd7* and 5′-CCGTCAGAATACACACGGAAT-3′ (p63 KD1) and 5′-

CCCAGTATGTAGAAGATCCTA-3′ (p63 KD2) for *p63* respectively. Control plasmid containing scrambled shRNA sequence was purchased from Sigma-Aldrich. For isoform specific knockdown studies in mouse, the targeting shRNA sequences are: 5′-GGCACCTGAATTCTGTTA-3′ for Δ*Np63* KD1, 5′-GCACCTGAATTCTGTTAT-3′ for Δ*Np63* KD2, 5′-GGTTACTTGAAGACTCTTA-3′ for TAp63 *KD1* and 5′-CCCATCTGTTGGTATCAAA-3′ for TAp63 *KD2*.

For general and isoform-specific p63 knockdown studies in human cells, the targeting shRNA sequences are: 5′-CCCAGTATGTAGAAGATCCTA-3′ for *p63*, 5′-GCAGCATTGATCAATCTTA-3′ for Δ*Np63*, 5′-CGACAAACAAGATTGAGATTA-3′ for *TAp63*, 5′-GGGAACAGCCATGCCCAGTATG-3′ for *p63* DBD, and 5′-CCGGCTGTTCGTCTACCTCTTCAT-3′ for *FZD7*.

Viral production and infection

For lentivirus-mediated overexpression or knockdown studies, expression plasmids and shRNA constructs are described above. All plasmids were packaged into virus using HEK293-T cells as packaging cell lines and helper plasmids VSVG and dR8.9 following standard protocols. Primary cells were spin infected with virus-containing media supplemented with 2 μg/mL polybrene for 2 hours at 1000 g at 4°C and then either plated in matrigel or transplanted. Self renewal activity of transduced MaSCs after transplantation was tested by their ability to regenerate functional mammary glands in virgin and pregnant mouse as shown in Supplementary Figure 1c. For HMLE cells, virally infected cells were selected with puromycin. The retroviral vectors were transfected into H29 packaging cell line. Viruses were collected 48–72 hrs after transfection. Cells were infected with viral media in presence of 5 μg/mL polybrene. The infected cells were selected with puromycin.

Luciferase enhancer reporter assay

HMLE or iMMEC cells were seeded in 24-well plates 24h prior to transfection. The following day, 600 ng of the WT-ΔNp63, MT-ΔNp63 and WT-TA-p63 expression plasmids were co-transfected along with 400 ng enhancer reporter plasmid (*FZD7* enhancer or *TK* control) and 100 ng of internal control plasmid that constitutively expressing renilla-luciferase using Lipofectamine 2000 (Invitrogen). Cells were collected 24h post-transfection and assayed for luciferase activity using the Glomax 96 microplate luminometer (Promega).

Wnt reporter assay

P4 cells were co-transduced with the 7TFC Wnt reporter[68] and either control, ΔNp63 or TAp63 virus and then plated on gelatin. After 48 h, cells were treated with Wnt3A (R & D systems) for 24 h. Cells were then selected for infected cells by sorting for mCherry and luciferase assay was performed as previously described[68]. MDA-MB-231 cells were co-transduced with the 7TFC Wnt reporter[68] and either control, ΔNp63 KD, TAp63 KD or Fzd7 KD virus and then plated. Luciferase assay was performed using similar method to MaSCs.

Protein extraction and western blot analysis

Proteins were extracted from primary epithelial cell cultures and cell lines in RIPA buffer as previously described[10]. Western blot analysis was performed using standard protocol. Antibodies and dilutions used are listed in Supplementary Table 2.

Histological analysis, immunohistochemistry and immunofluorescence

For histological analysis, mammary gland specimens were processed as previously described[10]. Antibodies and dilutions used are listed in the Supplementary Table 2. DAPI was used to stain nuclei. Confocal images were taken using Nikon A1 confocal microscope.

Immunohistochemical analysis of breast tumor specimens

Normal mammary tissues and breast tumor specimens used in the study were de-identified samples and were considered exempt by Institutional Review Boards of Princeton University and the Rutgers New Jersey Medical School, as well as the Area Vasta Romagna Ethics Committee (CEIIAV IRST IRCCS), Meldola, Italy. Immunohistochemistry of ΔNp63 and FZD7 was performed by the Tissue Analytic Core Facility in the Rutgers Cancer Institute of New Jersey. Anti-ΔNp63, anti-TAp63 and Anti-FZD7 (Sigma-Aldrich, Cat # AV41251) were first optimized on regular human breast tissue slides using a Ventana Medical Systems Discovery XT automated immunostainer. Slides were processed as previously described[10]. Anti-ΔNp63, anti-TAp63 and anti-FZD7 antibody were applied at dilutions of 1:80, 1:80 and 1:100 respectively and incubated at room temperature for two hours. 12 primary human breast tumor samples were used for immunohistological staining in our ΔNp63/FZD7 expression correlation study. Each sample was scored as negative (0), low (1), medium (2), or high (3) according to ΔNp63 and FZD7 staining abundance. A tumor with a mean score larger than 1 was considered to be positive for the expression of the gene. Pearson's coefficient test was performed to assess statistical significance.

qRT-PCR analyses

Total RNA was isolated from primary cells using Qiagen RNA extraction kit in accordance with the manufacturer's instructions. Real-time RT-PCR was performed on an ABI 7900 96 HT series PCR machine (Applied Biosystem) using SYBR Green Supermix (Bio-Rad Laboratories). The gene-specific primer sets were used at a final concentration of 0.2 μM and their sequences are listed in Supplementary Table 3. All qRT-PCR assays were performed in duplicate in at least three independent experiments using three different tissue samples.

Microarray analysis

The P4, P5, P6 subpopulations of mammary epithelial cells (MECs) were isolated from the mammary glands (4 mammary glands from each group) of virgin mice. MECs were isolated using FACS as described in[32]. The unsorted whole MECs or sorted P4 cells from WT and $\Delta Np63^{gfp/+}$ mice (C57/B6 strain) at 7 weeks age were prepared as described. RNA was collected from these samples using the RNAeasy Mini Kit (Qiagen, Valencia VA) according to manufacturer's instructions. The gene expression profiles of various populations of MECs from the wild type and $\Delta Np63^{gfp/+}$ mice were determined using Agilent mouse GE 4x44k

two-color microarrays system (Agilent, G4122F), following the manufacturer's instructions. Briefly, the RNA samples and universal mouse reference RNA (Agilent 740100) were labeled with CTP-cy5 and CTP-cy3, respectively, using the Agilent Quick Amp Labeling Kit. Labeled testing and reference RNA samples were mixed in equal proportions, and hybridized to the mouse GE 4x44K array. The arrays were scanned with an Agilent G2565BA scanner and raw data was extracted using Agilent Feature Extraction software (v9.5). Data was analyzed using the GeneSpring GX software (Agilent). The expression value of individual probes refers to the Log2(Cy5/Cy3) ratio.

Gene set enrichment analysis (GSEA)

GSEA v2.0 was used to perform the GSEA on various functional and/or characteristic gene signatures as described in previous study[10]. Normalized microarray expression data were rank-ordered by differential expression between cell populations and/or genetic background as indicated, using the provided ratio of classes (i.e., fold change) metric. Two independent MaSC specific gene signatures were used to characterize MaSC characteristics. Both are defined by significantly upregulated genes ($p < 0.05$ and $FC > 3$) in MaSC-enriched subpopulations from MECs of wild type mice. Among which, the "MaSC signature from current study" is derived from the microarray data collected from our lab as described in this study (GSE47493). The genes qualify by showing >3 folds upregulation in P4 comparing to both P5 and P6 of wild type mice. The other MaSC signature is derived from published dataset GSE22446. Other gene signatures used in GSEA were obtained from the MSigDB database v3.0 (September 2010 release).

Clinical dataset analysis

To develop conserved gene expression readout for ΔNp63 activity, we first interrogated microarray datasets comparing both MECs as well as the MaSC enriched (P4) subpopulation of WT and $\Delta Np63^{gfp+/-}$ mice. Using log_2-transformed and median centered microarray data, we defined the ΔNp63 signature as the gene expression values of all genes with > 1.5-fold changes between MECs and P4 cells compared their corresponding wild-type control cells. This corresponded to 125 genes up- or downregulated in both MECs and P4 cells compared to wild type. To reduce each gene to one expression value, we took the average of its expression in MECs and in P4 cells. We then applied this signature to log_2-transformed and median centered microarray data from the EMC286 clinical breast cancer dataset[47]. To predict ΔNp63 activity in a given patient, we used overall Pearson correlation of patient gene expression values and ΔNp63 signature gene expression values for all genes in the experimentally-derived ΔNp63 signature. The Pearson correlation coefficient values were used as a given patient's ΔNp63 signature score. We then defined ΔNp63-high and ΔNp63-low patients as those with above and below median ΔNp63 signature scores, respectively.

To analyze the expression of different isoforms of p63 in breast cancer patients, we used the TCGA breast invasive carcinoma (BRCA) exon expression RNAseq dataset[46]. We downloaded the expression dataset (dataset ID TCGA_BRCA_exp_HiSeqV2_exon) and patient sample characteristics from the UCLA cancer browser (https://genome-cancer.ucsc.edu/proj/site/hgHeatmap/). The expression of isoform-specific exons were used to represent the expression of specific isoforms. The Pearson correlation coefficiency was

calculated to measure the correlation between genes. For grouping, 1 base unit RPKM (Reads Per Kilobase of exon model per Million mapped reads) were set as cutoff so less than 1 RPKM is defined as absent (or undetectable) and more than 1 RPKM is defined as present (or detectable).

In silico analysis

The sequence conservation between the mouse and human *FZd7* enhancer was examined using the VISTA computational tools for comparative genomics (http://genome.lbl.gov/vista/index.shtml).

Chromatin immunoprecipitation

HMEC cells (Lonza) or MMTV-Wnt-1 primary cells were grown to 80% confluence and cells were then cross-linked with 1% formaledyde and processed. The crosslinking, immunoprecipitation, washing, elution, reverse crosslinking, and proteinase K treatment were performed according to the manufacturer's directions described in the Magna ChIP G Chromatin Immunoprecipitation Kit from Millipore. Antibodies used were anti-4A4, H-129 (Santa Cruz) or normal rabbit IgG. Purified immunoprecipitated DNA was used for real time qPCR. Primers for ChIP PCR are: 5′-TATCAGCATTCCAGGCCCAC-3′ (forward) and 5′-TTCCTGGGAGAACAATCGCC-3′ (reverse) for human *FZD7*; 5′-AATGAGGCAAACACCCCCTC-3′ (forward) and 5′-CTCCGGGGGATTAAAGGTGG-3′ (reverse) for mouse *Fzd7*; 5′-CGAGATCCCTCCAAAATCAA (forward) and 5′-CCCAGCCTTCTCCATGG (reverse) for human *GAPDH* and 5′-AACATCAAATGGGGTGAGG-3′ (forward), 5′-GGCCTTCTCCATGGTGGT-3′ (reverse) for mouse *Gapdh*.

Statistical Analysis

Results were generally reported as mean ± SD (standard deviation) as indicated in the figure legend. For comparisons of central tendencies, normally distributed datasets were analyzed using unpaired (with the exception of analyses of cellular populations from paired contralateral injections) two-sided Student's t-tests under assumption of equal variance. Non-normally distributed datasets were analyzed using non–parametric Mann-Whitney U tests. Pearson's Chi-squared tests were used for tumor incidence using ELDA software. To adjust for host effects, paired two-sided Student's t-tests assuming equal variance were used for experiments in which cellular populations were compared following matched contralateral injections of control and experimental cell types into the same mouse (Supplementary Fig. 3g only). For tumor-free survival analyses, data were displayed as Kaplan-Meier plots and significance was assessed by log-rank tests. Statistical analyses specific to Limiting Dilution Assays and Gene Set Enrichment Analysis are described above. All the experiments with representative images (including western blot, FACS plot, histology and immunofluorescence) have been repeated at least three times and representative images were shown.

Supplementary Material

Refer to Web version on PubMed Central for supplementary material.

Acknowledgments

We thank our lab members for helpful discussions, Drs R.A. Weinberg and V. Karantza for iMMEC and HMLE cell lines, and Drs. A.L. Welm and M.T. Lewis for PDX lines, respectively. This research was supported by grants from the Brewster Foundation, the Department of Defense (BC123187) and the National Institutes of Health (R01CA134519 and R01CA141062) to Y.K. and from the Canadian Cancer Society Research Institute to C.J.E. R.C. and N.K. are recipients of postdoctoral fellowships from the Department of Defense and MITACS, respectively. This research was also supported by the Transgenic/Knockout, Tissue Analytic Service and Flow Cytometry Shared Resources of the Cancer Institute of New Jersey (P30CA072720).

References

1. Visvader JE. Cells of origin in cancer. Nature. 2011; 469:314–322. [PubMed: 21248838]
2. Nguyen LV, Vanner R, Dirks P, Eaves CJ. Cancer stem cells: an evolving concept. Nature reviews. Cancer. 2012; 12:133–143.
3. Visvader JE, Lindeman GJ. Cancer stem cells: current status and evolving complexities. Cell stem cell. 2012; 10:717–728. [PubMed: 22704512]
4. Magee JA, Piskounova E, Morrison SJ. Cancer stem cells: impact, heterogeneity, and uncertainty. Cancer cell. 2012; 21:283–296. [PubMed: 22439924]
5. Lessard J, Sauvageau G. Bmi-1 determines the proliferative capacity of normal and leukaemic stem cells. Nature. 2003; 423:255–260. [PubMed: 12714970]
6. Maddox J, et al. Transcription factor Oct1 is a somatic and cancer stem cell determinant. PLoS genetics. 2012; 8:e1003048. [PubMed: 23144633]
7. Cicalese A, et al. The tumor suppressor p53 regulates polarity of self-renewing divisions in mammary stem cells. Cell. 2009; 138:1083–1095. [PubMed: 19766563]
8. Guo W, et al. Slug and Sox9 cooperatively determine the mammary stem cell state. Cell. 2012; 148:1015–1028. [PubMed: 22385965]
9. Kouros-Mehr H, et al. GATA-3 links tumor differentiation and dissemination in a luminal breast cancer model. Cancer cell. 2008; 13:141–152. [PubMed: 18242514]
10. Chakrabarti R, et al. Elf5 inhibits the epithelial-mesenchymal transition in mammary gland development and breast cancer metastasis by transcriptionally repressing Snail2. Nature cell biology. 2012; 14:1212–1222. [PubMed: 23086238]
11. Crum CP, McKeon FD. p63 in epithelial survival, germ cell surveillance, and neoplasia. Annual review of pathology. 2010; 5:349–371.
12. Yang A, et al. p63, a p53 homolog at 3q27–29, encodes multiple products with transactivating, death-inducing, and dominant-negative activities. Molecular cell. 1998; 2:305–316. [PubMed: 9774969]
13. Su X, Chakravarti D, Flores ER. p63 steps into the limelight: crucial roles in the suppression of tumorigenesis and metastasis. Nature reviews. Cancer. 2013; 13:136–143.
14. Deyoung MP, Ellisen LW. p63 and p73 in human cancer: defining the network. Oncogene. 2007; 26:5169–5183. [PubMed: 17334395]
15. Flores ER, et al. Tumor predisposition in mice mutant for p63 and p73: evidence for broader tumor suppressor functions for the p53 family. Cancer cell. 2005; 7:363–373. [PubMed: 15837625]
16. Keyes WM, et al. p63 heterozygous mutant mice are not prone to spontaneous or chemically induced tumors. Proceedings of the National Academy of Sciences of the United States of America. 2006; 103:8435–8440. [PubMed: 16714381]
17. Guo X, et al. TAp63 induces senescence and suppresses tumorigenesis in vivo. Nature cell biology. 2009; 11:1451–1457. [PubMed: 19898465]
18. Su X, et al. TAp63 suppresses metastasis through coordinate regulation of Dicer and miRNAs. Nature. 2010; 467:986–990. [PubMed: 20962848]
19. Karni-Schmidt O, et al. Distinct expression profiles of p63 variants during urothelial development and bladder cancer progression. The American journal of pathology. 2011; 178:1350–1360. [PubMed: 21356385]

20. Keyes WM, et al. DeltaNp63alpha is an oncogene that targets chromatin remodeler Lsh to drive skin stem cell proliferation and tumorigenesis. Cell stem cell. 2011; 8:164–176. [PubMed: 21295273]
21. DiRenzo J, et al. Growth factor requirements and basal phenotype of an immortalized mammary epithelial cell line. Cancer research. 2002; 62:89–98. [PubMed: 11782364]
22. Teuliere J, et al. Targeted activation of beta-catenin signaling in basal mammary epithelial cells affects mammary development and leads to hyperplasia. Development. 2005; 132:267–277. [PubMed: 15590737]
23. Li N, et al. Reciprocal intraepithelial interactions between TP63 and hedgehog signaling regulate quiescence and activation of progenitor elaboration by mammary stem cells. Stem cells. 2008; 26:1253–1264. [PubMed: 18292212]
24. Regan JL, et al. c-Kit is required for growth and survival of the cells of origin of Brca1-mutation-associated breast cancer. Oncogene. 2012; 31:869–883. [PubMed: 21765473]
25. Yalcin-Ozuysal O, et al. Antagonistic roles of Notch and p63 in controlling mammary epithelial cell fates. Cell death and differentiation. 2010; 17:1600–1612. [PubMed: 20379195]
26. Laurikkala J, et al. p63 regulates multiple signalling pathways required for ectodermal organogenesis and differentiation. Development. 2006; 133:1553–1563. [PubMed: 16524929]
27. Barton CE, et al. Novel p63 target genes involved in paracrine signaling and keratinocyte differentiation. Cell death & disease. 2010; 1:e74. [PubMed: 21151771]
28. Wu N, Rollin J, Masse I, Lamartine J, Gidrol X. p63 regulates human keratinocyte proliferation via MYC-regulated gene network and differentiation commitment through cell adhesion-related gene network. The Journal of biological chemistry. 2012; 287:5627–5638. [PubMed: 22184109]
29. Caserta TM, et al. p63 overexpression induces the expression of Sonic Hedgehog. Molecular cancer research: MCR. 2006; 4:759–768. [PubMed: 17050669]
30. Reya T, Morrison SJ, Clarke MF, Weissman IL. Stem cells, cancer, and cancer stem cells. Nature. 2001; 414:105–111. [PubMed: 11689955]
31. Takebe N, Harris PJ, Warren RQ, Ivy SP. Targeting cancer stem cells by inhibiting Wnt, Notch, and Hedgehog pathways. Nature reviews. Clinical oncology. 2011; 8:97–106.
32. Shackleton M, et al. Generation of a functional mammary gland from a single stem cell. Nature. 2006; 439:84–88. [PubMed: 16397499]
33. van Amerongen R, Bowman AN, Nusse R. Developmental stage and time dictate the fate of Wnt/beta-catenin-responsive stem cells in the mammary gland. Cell stem cell. 2012; 11:387–400. [PubMed: 22863533]
34. Zeng YA, Nusse R. Wnt proteins are self-renewal factors for mammary stem cells and promote their long-term expansion in culture. Cell stem cell. 2010; 6:568–577. [PubMed: 20569694]
35. Reya T, Clevers H. Wnt signalling in stem cells and cancer. Nature. 2005; 434:843–850. [PubMed: 15829953]
36. de La Coste A, et al. Somatic mutations of the beta-catenin gene are frequent in mouse and human hepatocellular carcinomas. Proc Natl Acad Sci U S A. 1998; 95:8847–8851. [PubMed: 9671767]
37. Klaus A, Birchmeier W. Wnt signalling and its impact on development and cancer. Nature reviews. Cancer. 2008; 8:387–398.
38. Smid M, et al. Subtypes of breast cancer show preferential site of relapse. Cancer research. 2008; 68:3108–3114. [PubMed: 18451135]
39. Khramtsov AI, et al. Wnt/beta-catenin pathway activation is enriched in basal-like breast cancers and predicts poor outcome. The American journal of pathology. 2010; 176:2911–2920. [PubMed: 20395444]
40. Howe LR, Brown AM. Wnt signaling and breast cancer. Cancer biology & therapy. 2004; 3:36–41. [PubMed: 14739782]
41. Alexander CM, Goel S, Fakhraldeen SA, Kim S. Wnt signaling in mammary glands: plastic cell fates and combinatorial signaling. Cold Spring Harbor perspectives in biology. 2012; 4
42. Vaillant F, et al. The mammary progenitor marker CD61/beta3 integrin identifies cancer stem cells in mouse models of mammary tumorigenesis. Cancer research. 2008; 68:7711–7717. [PubMed: 18829523]

43. Romano RA, et al. DeltaNp63 knockout mice reveal its indispensable role as a master regulator of epithelial development and differentiation. Development. 2012; 139:772–782. [PubMed: 22274697]
44. Kouwenhoven EN, et al. Genome-wide profiling of p63 DNA-binding sites identifies an element that regulates gene expression during limb development in the 7q21 SHFM1 locus. PLoS genetics. 2010; 6:e1001065. [PubMed: 20808887]
45. Karantza-Wadsworth V, White E. A mouse mammary epithelial cell model to identify molecular mechanisms regulating breast cancer progression. Methods in enzymology. 2008; 446:61–76. [PubMed: 18603116]
46. Cancer Genome Atlas N. Comprehensive molecular portraits of human breast tumours. Nature. 2012; 490:61–70. [PubMed: 23000897]
47. Wang Y, et al. Gene-expression profiles to predict distant metastasis of lymph-node-negative primary breast cancer. Lancet. 2005; 365:671–679. [PubMed: 15721472]
48. DeRose YS, et al. Tumor grafts derived from women with breast cancer authentically reflect tumor pathology, growth, metastasis and disease outcomes. Nature medicine. 2011; 17:1514–1520.
49. Herschkowitz JI, et al. Identification of conserved gene expression features between murine mammary carcinoma models and human breast tumors. Genome biology. 2007; 8:R76. [PubMed: 17493263]
50. Lim E, et al. Transcriptome analyses of mouse and human mammary cell subpopulations reveal multiple conserved genes and pathways. Breast cancer research: BCR. 2010; 12:R21. [PubMed: 20346151]
51. Cho RW, et al. Isolation and molecular characterization of cancer stem cells in MMTV-Wnt-1 murine breast tumors. Stem cells. 2008; 26:364–371. [PubMed: 17975224]
52. Carroll DK, et al. p63 regulates an adhesion programme and cell survival in epithelial cells. Nature cell biology. 2006; 8:551–561. [PubMed: 16715076]
53. Makarem M, et al. Developmental changes in the in vitro activated regenerative activity of primitive mammary epithelial cells. PLoS biology. 2013; 11:e1001630. [PubMed: 23966837]
54. Balboni AL, et al. DeltaNp63alpha-mediated activation of bone morphogenetic protein signaling governs stem cell activity and plasticity in normal and malignant mammary epithelial cells. Cancer research. 2013; 73:1020–1030. [PubMed: 23243027]
55. Metzger-Filho O, et al. Dissecting the heterogeneity of triple-negative breast cancer. Journal of clinical oncology: official journal of the American Society of Clinical Oncology. 2012; 30:1879–1887. [PubMed: 22454417]
56. Watson CJ, Gusterson BA. A prophylactic vaccine for breast cancer? Breast cancer research: BCR. 2010; 12:310. [PubMed: 20828424]
57. Lehmann BD, et al. Identification of human triple-negative breast cancer subtypes and preclinical models for selection of targeted therapies. The Journal of clinical investigation. 2011; 121:2750–2767. [PubMed: 21633166]
58. Yang L, et al. FZD7 has a critical role in cell proliferation in triple negative breast cancer. Oncogene. 2011; 30:4437–4446. [PubMed: 21532620]
59. King TD, Zhang W, Suto MJ, Li Y. Frizzled7 as an emerging target for cancer therapy. Cellular signalling. 2012; 24:846–851. [PubMed: 22182510]
60. Kinzler KW, Vogelstein B. Lessons from hereditary colorectal cancer. Cell. 1996; 87:159–170. [PubMed: 8861899]
61. Molyneux G, Smalley MJ. The cell of origin of BRCA1 mutation-associated breast cancer: a cautionary tale of gene expression profiling. Journal of mammary gland biology and neoplasia. 2011; 16:51–55. [PubMed: 21336547]
62. Lim E, et al. Aberrant luminal progenitors as the candidate target population for basal tumor development in BRCA1 mutation carriers. Nature medicine. 2009; 15:907–913.
63. Eirew P, et al. A method for quantifying normal human mammary epithelial stem cells with in vivo regenerative ability. Nature medicine. 2008; 14:1384–1389.
64. Asselin-Labat ML, et al. Control of mammary stem cell function by steroid hormone signalling. Nature. 2010; 465:798–802. [PubMed: 20383121]

65. Kannan, N., et al. Glutathione-dependent and -independent oxidative stress-control mechanisms distinguish normal human mammary epithelial cell subsets. Proceedings of the National Academy of Sciences of the United States of America; 2014;

66. Matveeva OV, et al. Optimization of duplex stability and terminal asymmetry for shRNA design. PloS one. 2010; 5:e10180. [PubMed: 20422034]

67. Brummelkamp TR, Bernards R, Agami R. Stable suppression of tumorigenicity by virus-mediated RNA interference. Cancer cell. 2002; 2:243–247. [PubMed: 12242156]

68. Fuerer C, Nusse R. Lentiviral vectors to probe and manipulate the Wnt signaling pathway. PloS one. 2010; 5:e9370. [PubMed: 20186325]

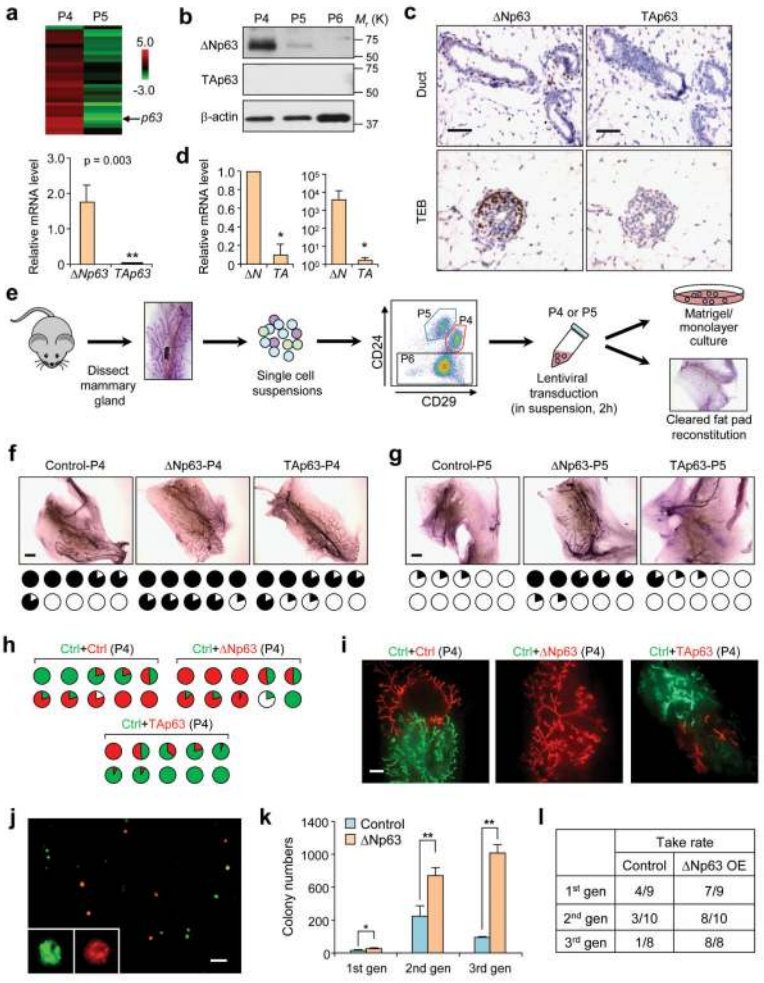

Figure 1. ΔNp63 is enriched in MaSCs and promote MaSC activity

(a) Heat map of differential expression of 26 transcriptional regulators, including p63 (arrow), in different mouse MEC subpopulations (upper panel). qRT-PCR analysis of Δ*Np63* and *TAp63* mRNAs in MECs (lower panel) (n = 3 samples; data represents mean ± s.d.). qRT-PCR values were normalized to *Gapdh*. **(b)** Immunoblot of ΔNp63 expression in different mouse MEC subpopulations. **(c)** Immunohistochemical analysis of ΔNp63 and TAp63 expression in the terminal end buds (TEBs) and ducts of mammary gland serial sections. **(d)** qRT-PCR analysis of Δ*Np63* and *TAp63* mRNAs in normal human mammary epithelium (left panel, n = 3 samples; data represents mean ± s.d.) and $CD49f^{hi}EpCAM^{neg/low}$ MaSC-enriched population[63] (right panel, n = 3 samples; data represents mean ± s.d.). qRT-PCR values were normalized to *GAPDH*. *p < 0.05 by Student's t test. **(e)** Strategy of lentiviral transduction of different MEC subpopulations. **(f)** MaSC-enriched $Lin^{-}CD24^{+}CD29^{hi}$ (P4) population was isolated and transduced with indicated lentivirus constructs and transplanted into cleared fat pads (1000 cells). **(g)** 1000 luminal cells ($Lin^{-}CD24^{+}CD29^{lo}$) (P5) were transduced with indicated lentivirus constructs and injected to cleared fat pad. Representative mammary outgrowths shown in **f** and **g**. In pie graph below representative images, each circle represents one mammary gland, with blackened area representing the degree of gland filling with outgrowth. ● 80–100%, ◕ 30–

80%, ◔ 0–30% and no reconstitution. **(h, i)** Pie graph (**h**) and representative fluorescence images (**i**) of the mammary fat pads after competitive reconstitution assay. **(j)** Representative images of 3-D matrigel colonies of P4 population from GFP and dsRED MECs mixed equally. **(k)** Number of colonies formed in three generations in 3-D matrigel assay (n = 3 samples; data represents mean ± s.d.). **(l)** Table showing reconstitution rate of the mammary gland over successive generations after transplantation of 10,000 unsorted MECs transduced with control or ΔNp63 expressing lentiviruses. *$p < 0.05$, **$p < 0.01$ by Student's t test. Size bar, 40 μm in **c**, 1 mm in **f** and **g**, 2mm in **i,** and 3mm in **j**. Uncropped images of blots are shown in Supplementary Fig. 9.

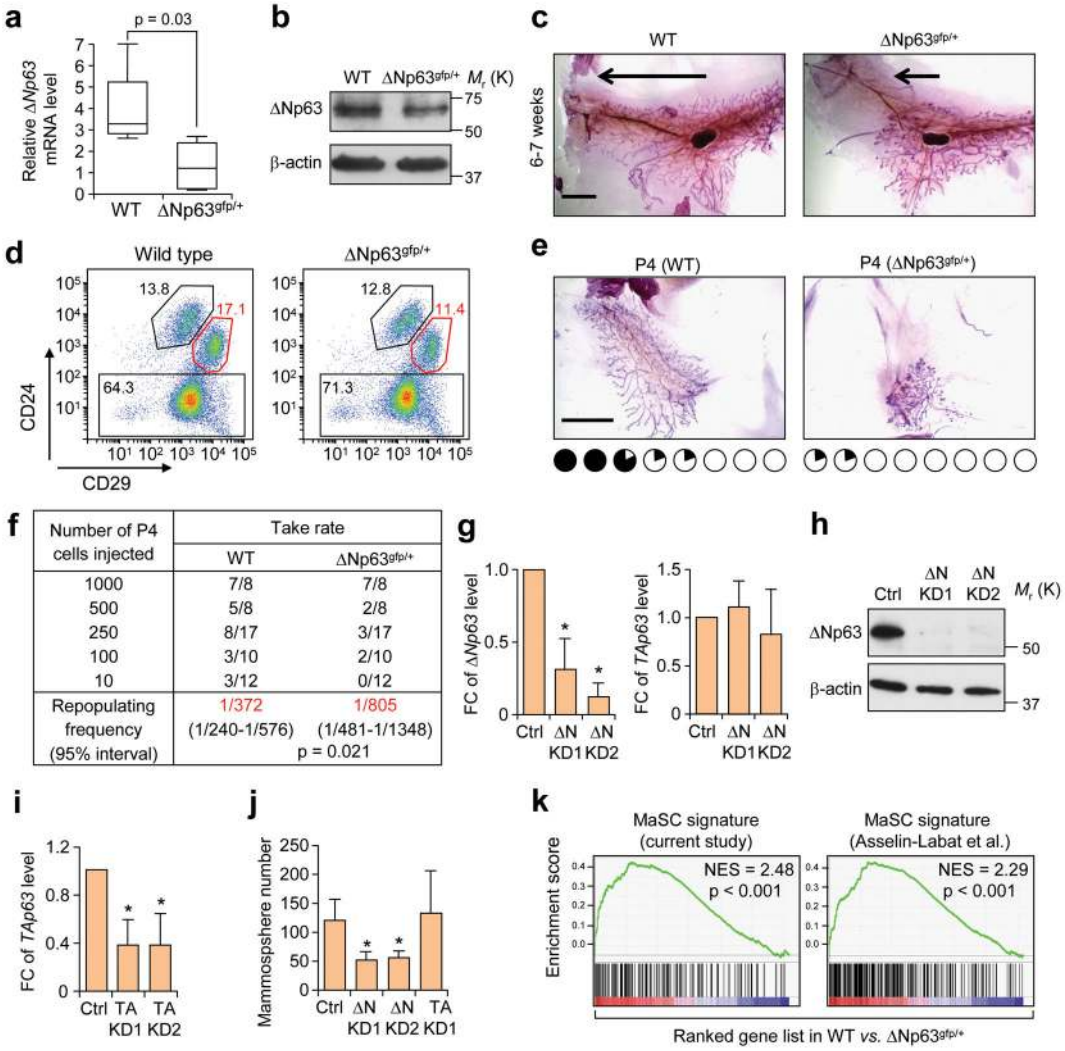

Figure 2. ΔNp63 deficiency reduces MaSC activity

(a, b) Box plot **(a)** and western blot **(b)** of ΔNp63 expression in P4 cells from WT and ΔNp63$^{gfp/+}$ mice. Boxes in **a** represents 75th, 50th and 25th percentile of the values. Top and bottom lines represent maximum and minimal data points within 1.5x IQ (inter quarter) range, respectively. P value computed by Mann Whitney U test (n = 5 samples per genotype). **(c)** Representative mammary outgrowths from WT and ΔNp63$^{gfp/+}$ mice. **(d)** Representative FACS profiles of MECs from WT and ΔNp63$^{gfp/+}$ mouse. **(e)** Representative mammary outgrowths from **f**. Each circle below the images represents one mammary gland, with blackened area representing the degree of gland filling with outgrowth. 80–100%, ● 30–80%, ◔ 0–30% and no reconstitution. **(f)** Table showing transplantation of limiting numbers of P4 cells into cleared mammary fat pads from indicated mice (n= number of mammary fat pad injections as indicated in the table). P value was obtained by Pearson's Chi-squared test using ELDA software. **(g)** Fold change (FC) of Δ*Np63* mRNA level in primary MECs transduced with control and two ΔNp63 shRNA lentiviral constructs (ΔN KD1 and ΔN KD2) (left panel). Fold change of *TAp63* mRNA level in control or ΔNp63-KD MECs (right panel). **(h)** Western blot of ΔNp63 in control and ΔNp63 KD MECs. **(i)**

Fold change of *TAp63* mRNA level in primary MECs transduced with control and two TAp63 shRNA lentiviral constructs. TA isoform-specific KD of TAp63 was confirmed by qRT-PCR since TAp63 protein is undetectable in MECs. **(j)** Quantification of mammosphere formed by control, ΔNp63-KD and TAp63-KD P4 cells (20,000 cells) from WT mice mammary gland. In **g**, **i** and **j**, n = 3 samples; data represents mean ± s.d. *$p < 0.05$ by Student's t test. **(k)** GSEA demonstrating enrichment of MaSC gene signatures in WT versus $\Delta Np63^{gfp/+}$ MECs using MaSC signatures derived from the current study (left panel) or a previously reported MaSC gene signature[64] (right panel). Size bar, 2 mm and 4 mm in **c** and **e** respectively. Uncropped images of blots are shown in Supplementary Fig. 9.

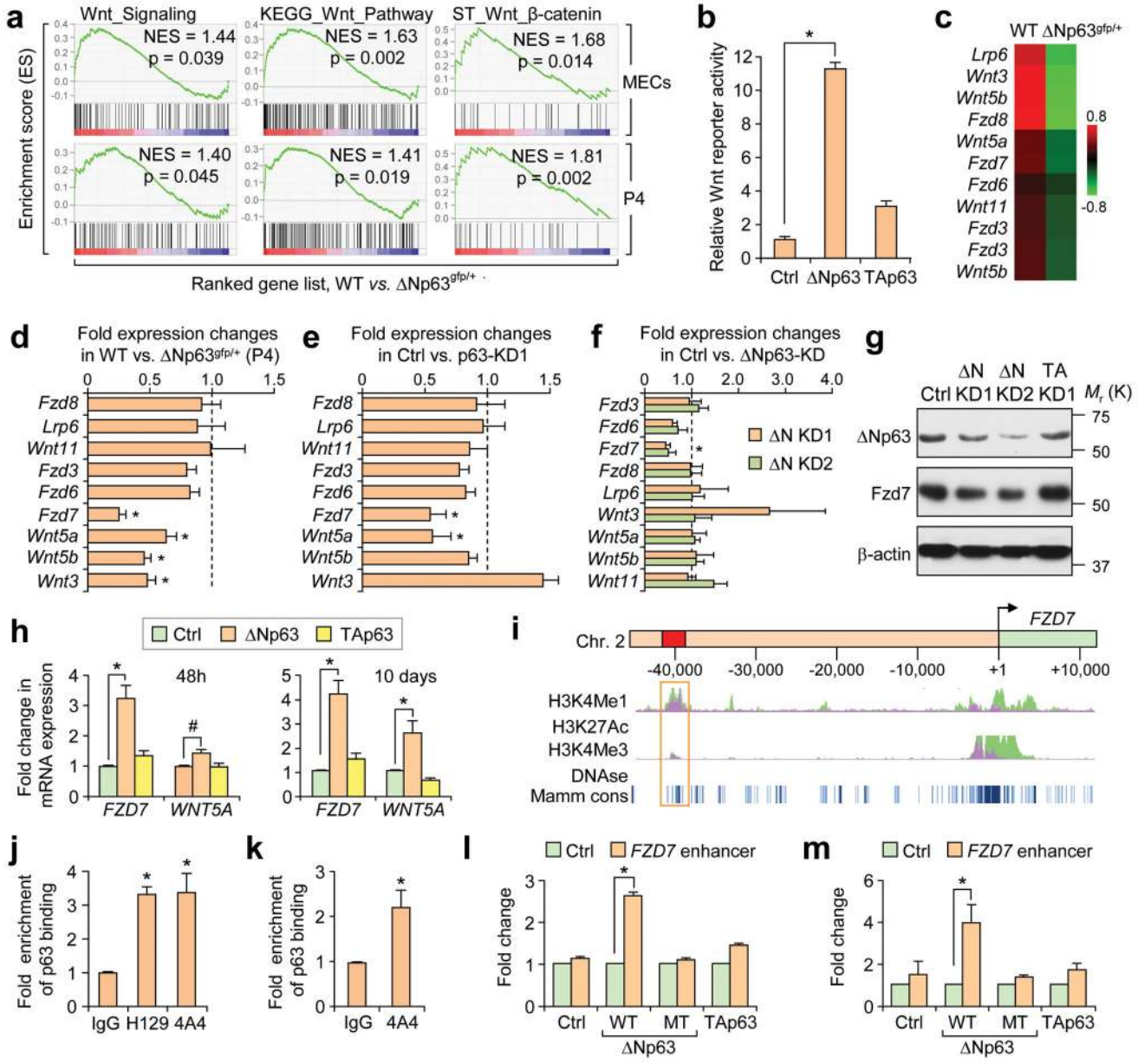

Figure 3. ΔNp63 but not TAp63 increases Wnt signaling via direct activation of *Fzd7* expression

(a) GSEA of Wnt gene signatures in unsorted (upper panels) or P4 (lower panels) WT versus ΔNp63$^{gfp/+}$ MECs. **(b)** Relative expression of Wnt luciferase reporter in P4 cells after lentiviral transduction of vector control, ΔNp63 or TAp63 lentiviruses (n = 3 samples; data represents mean ± s.d.). **(c, d)** Heat map of microarray data **(c)** and qRT-PCR **(d)** showing the expression of Wnt pathway genes in wild type and ΔNp63$^{gfp/+}$ P4 cells from 7 week-old virgin mice. **(e)** qRT-PCR analysis of the Wnt signaling genes in control or p63-KD primary MECs. **(f)** qRT-PCR analysis of the Wnt signaling genes in control or ΔNp63 KD MECs. In **d–f**, n = 3 samples; data represents mean ± s.d. **(g)** Western blot analysis of ΔNp63 and Fzd7 in control, ΔNp63 and TAp63 KD MECs. **(h)** qRT-PCR analysis of the expression of *FZD7* and *WNT5A* in control, ΔNp63, or TAp63 overexpressing HMLE cells at 48 h (n = 3

samples) or 10 days (n = 6 technical replicates pooled from 2 independent experiments) post-infection. Real time values were normalized to the housekeeping gene *GAPDH*. Data represents mean ± s.d. **(i)** ChIP-seq data from human keratinocytes show ΔNp63 binding region to a putative *FZD7* enhancer. Dnase: DNAse I hypersensitive sites. Mamm cons: mammalian conserved areas. **(j)** ChIP analysis of p63 (using H129 and 4A4 antibody) binding to the *FZD7* enhancer in HMEC (n = 3 samples; data represents mean ± s.d.). **(k)** ChIP analysis of p63 binding to *Fzd7* enhancer in MMTV-Wnt1 primary mammary tumor cells (n = 6 technical repeats pooled from 2 independent experiments; data represents mean ± s.d.). **(l, m)** Relative expression of *FZD7* enhancer-driven luciferase reporter in HMLE (**l**) and iMMEC (**m**) cells transiently transfected with indicated expression plasmids (n = 3 samples, data represents mean ± s.d.). *p < 0.05 by Student's t test. Uncropped images of blots are shown in Supplementary Fig. 9.

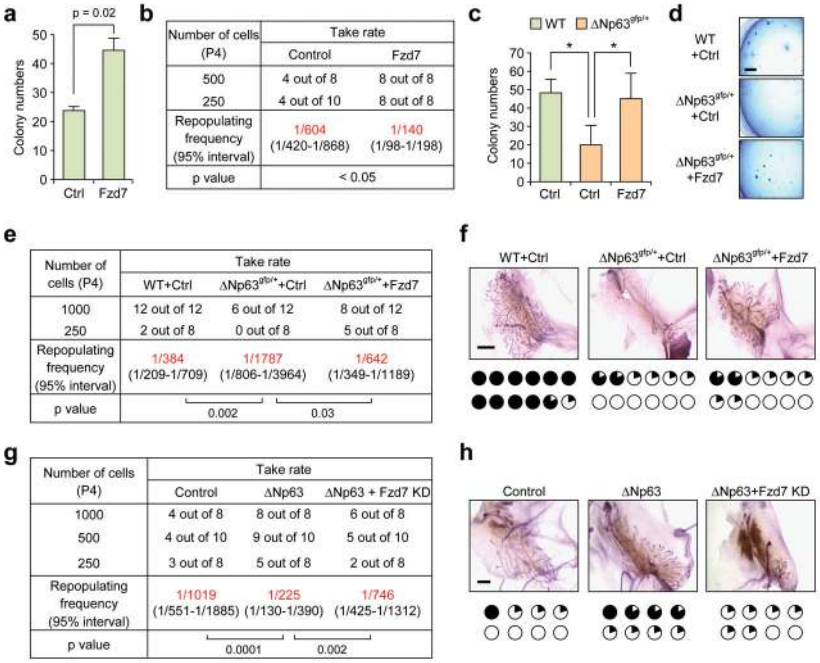

Figure 4. ΔNp63-mediated MaSC function is dependent on Fzd7

(a) Quantification of colonies formed by P4 cells transduced with indicated lentiviruses (n = 3 samples; data represents mean ± s.d.). **(b)** P4 cells were transduced with control or Fzd7 lentiviruses and limiting numbers of cells were transplanted into cleared fat pads. Table shows take rate quantifications. **(c)** Quantification of colonies formed by P4 cells from WT and ΔNp63$^{gfp/+}$ mice with or without Fzd7 overexpression (n = 5 samples; data represents mean ± s.d.). **(d)** Representative images of colonies from **c. (e)** Table showing reconstitution efficiency at limiting dilution of P4 cells from WT and ΔNp63$^{gfp/+}$ mice with Fzd7 overexpression. **(f)** Representative images and pie graph summary of outgrowths from **e. (g)** Table showing reconstitution efficiency at limiting dilution of P4 cells from control and ΔNp63 overexpressing cells with or without Fzd7 KD. **(h)** Representative images and pie graph summary of outgrowths from **g**. ● 80–100%, ◕ 30–80%, ◔ 0–30% and ○ No reconstitution. *p < 0.05 by Student's t test in **a** and **c**. In **b**, **e**, and **g**, n= number of mammary fat pad injections as indicated in tables. p value was obtained by Pearson's Chi-squared test using ELDA software. Size bar, 1 mm in **d** and **f**, and 2 mm in **h,** respectively.

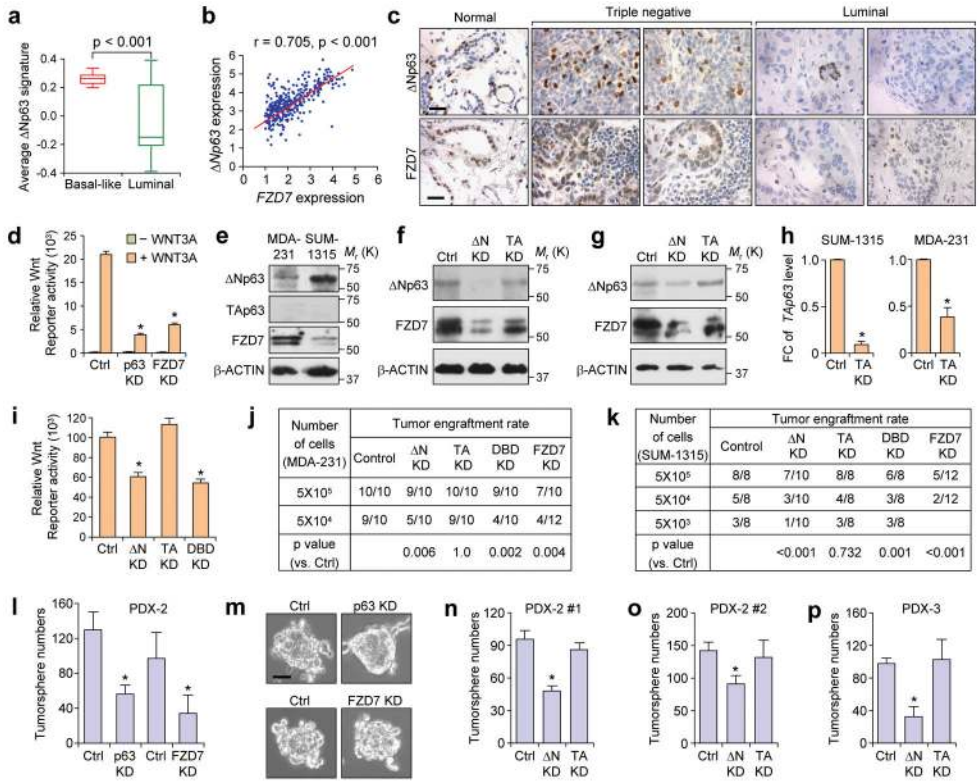

Number of cells (MDA-231)	Tumor engraftment rate				
	Control	ΔN KD	TA KD	DBD KD	FZD7 KD
5X10⁵	10/10	9/10	10/10	9/10	7/10
5X10⁴	9/10	5/10	9/10	4/10	4/12
p value (vs. Ctrl)		0.006	1.0	0.002	0.004

Number of cells (SUM-1315)	Tumor engraftment rate				
	Control	ΔN KD	TA KD	DBD KD	FZD7 KD
5X10⁵	8/8	7/10	8/8	6/8	5/12
5X10⁴	5/8	3/10	4/8	3/8	2/12
5X10³	3/8	1/10	3/8	3/8	
p value (vs. Ctrl)		<0.001	0.732	0.001	<0.001

Figure 5. ΔNp63 expression positively correlates with FZD7 expression and Wnt signaling in human breast cancer

(a) Δ*Np63* expression in clinical samples of basal and luminal type human tumors. Box represents 75th, 50th and 25th percentile of the values. Top and bottom lines represent maximum and minimal data points within 1.5x IQ (inter quarter) range, respectively (n = 286 tumors). **(b)** Scatter plot showing correlation between Δ*Np63* and *FZD7* expression in breast tumors from the TCGA-BRCA-RNAseqV2 dataset[46] (n = 1000 tumors). **(c)** IHC analysis of ΔNp63 and FZD7 expression. **(d)** Relative expression of Wnt luciferase reporter in MDA-MB-231 cells after lentiviral transduction of a Wnt reporter (7TFC), together with indicated shRNAs. **(e)** Western blot of ΔNp63, TAp63 and FZD7 expression in MDA-MB-231 and SUM-1315 cells. **(f, g)** Western blot of ΔNp63 and FZD7 expression in MDA-MB-231 and SUM-1315 cells after transduction with indicated shRNAs. **(h)** Fold change of *TAp63* mRNA level in MDA-MB-231 cells and SUM-1315 cells respectively, after transduction with control and TAp63 shRNA. **(i)** Relative expression of Wnt luciferase reporter in MDA-MB-231 cells after lentiviral transduction of a Wnt reporter (7TFC), together with indicated shRNAs. In **d**, **h** and **i**, n = 3 samples, data represents mean ± s.d. **(j)** Tumor incidence of MDA-MB-231 cells expressing indicated shRNAs. **(k)** Tumor incidence of SUM-1315 cells expressing indicated shRNAs. In **j** and **k**, n= number of mammary fat pad injections as indicated in the table. P value was obtained by Pearson's Chi-squared test using ELDA software. **(l)** Quantification of tumorsphere formed by control, p63-KD and Fzd7-KD tumors (10,000 cells) from PDX-2 (HCI002)[48]. **(m)** Representative images of tumorspheres from **l. (n–p)** Quantification of tumorsphere formed by control, ΔNp63 KD and TAp63 KD cells (10,000 cells) from PDX-2 tumors (HCI002) **(n–o)** and PDX-3 tumors

(HCI009) **(p). In l, n–p,** n = 4 tumors; data represents mean ± s.d. *p < 0.05 by Student's t test. Size bar, 40 μm in **c** and **m** respectively. Uncropped images of blots are shown in Supplementary Fig. 9.

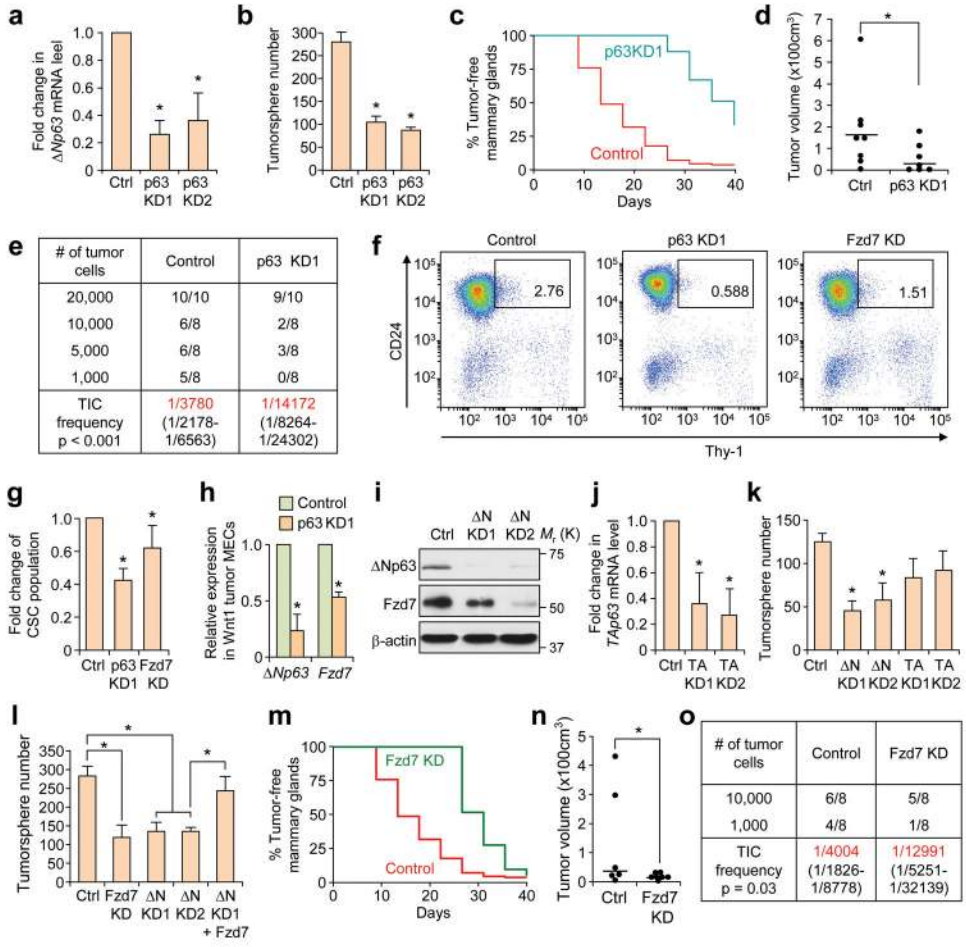

Figure 6. Loss of ΔNp63 attenuates tumor initiation in basal-like MMTV-Wnt1 tumors

(a) Fold change of Δ*Np63* mRNA level in primary MMTV-Wnt1 tumor MECs after transduction with indicated shRNAs (n = 3 tumors). **(b)** Quantification of tumorsphere numbers from MMTV-Wnt1 tumor cells transduced with indicated shRNAs (n = 3 tumors). **(c)** Kaplan-Meier curve of tumor-free mammary gland incidence using MMTV-Wnt1 tumor MECs (10,000 cells) transudced with indicated shRNAs. Log rank test was used for statistical analysis (n = 8 mice). **(d)** Average tumor volume at end point control (n = 8 tumors) and p63 KD1 (n = 7 tumors). **(e)** Tumor incidence of MMTV-Wnt1 tumor cells expressing the indicated shRNAs (). **(f)** Representative FACS profile of primary tumors. **(g)** Quantification of percentage of $CD45^{-}CD24^{+}Thy\text{-}1^{+}$ cells in control and p63-KD Wnt1 tumor cells as shown in **f** (n = 10 tumors). **(h)** qRT-PCR analysis of *Fzd7* and *p63* expression in control or p63-KD Wnt1 tumor MECs (n = 3 samples). **(i)** Western blot of ΔNp63 in control and ΔNp63-KD MMTV-Wnt1 tumor cells. **(j)** Fold change of *TAp63* mRNA level in MMTV-Wnt1 tumor cells after TAp63 KD (n = 3 tumors). **(k and l)** Quantification of tumorspheres formed by 10,000 MMTV-Wnt1 tumor cells transduced with indicated shRNAs (n = 3 tumors in **k** and n = 4 tumors in **l**). **(m)** Kaplan-Meier curve analysis of tumor-free mammary glands after injection of mice using control or Fzd7-KD MMTV-Wnt1 tumor MECs (10,000 cells). n = 8 mice. Log rank test was used for statistical

analysis. **(n)** Average tumor volume at end point (n = 6 tumors). **(o)** Tumor incidence of MMTV-Wnt1 tumor cells expressing the indicated shRNAs. In this figure, bar graph data represent mean ± s.d. *p < 0.05 by Student's t test in **a**, **b**, **h**, **j**, **k** and **l**. *p < 0.05 by Mann Whitney test in **d**, **g** and **n**. In **e** and **o**, n= number of mammary fat pad injections as indicated in the table. p value was obtained by Pearson's Chi-squared test using ELDA software. Uncropped images of blots are shown in Supplementary Fig. 9.

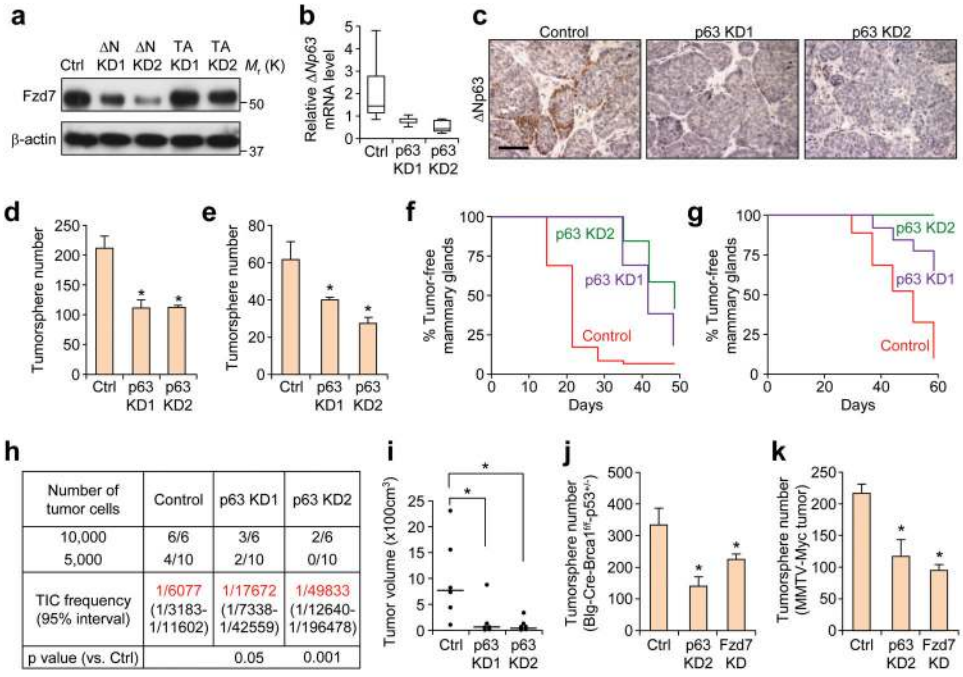

Number of tumor cells	Control	p63 KD1	p63 KD2
10,000	6/6	3/6	2/6
5,000	4/10	2/10	0/10
TIC frequency (95% interval)	1/6077 (1/3183-1/11602)	1/17672 (1/7338-1/42559)	1/49833 (1/12640-1/196478)
p value (vs. Ctrl)		0.05	0.001

Figure 7. Loss of ΔNp63 and Fzd7 attenuates tumor initiation in MMTV-Myc tumors

(a) Western blot analysis of Fzd7 expression in primary MMTV-Myc tumor cells transduced with indicated shRNAs. **(b, c)** Reduced level of ΔNp63 mRNA (**b**) and protein (**c**) expression in primary MMTV-Myc tumor cells with or without p63 KD. *p < 0.05 by Mann Whitney U test and n = 5 tumors per group in **b**. Box represents 75th, 50th and 25th percentile of the values. The top and bottom lines represent the maximum and minimal data points within 1.5x IQ (inter quarter) range, respectively. **(d, e)** Freshly isolated tumor MECs with or without p63 KD were used for tumorsphere assays in low adherent plates. Bar graphs show quantification of tumorsphere numbers in control and p63-KD MECs (10,000 cells) (n = 4 tumors; data represents mean ± s.d.). **(f, g)** Kaplan-Meier curves showing mammary gland tumor-free survival using MMTV-Myc tumor MECs transduced with control and p63 shRNAs (p63 KD1 and p63 KD2). 10,000 cells (n = 6 mice per group) and 5000 cells (n = 10 mice per group) were injected in **f** and **g,** respectively. Log rank test was used for statistical analysis and p values computed for both plots are < 0.001. **(h, i)** Tumor incidence (**h**) and volume (**i**) was calculated at end point. P value was obtained by Pearson's Chi-squared test using ELDA software in **h** (n= number of mammary fat pad injections as indicated in table). *p < 0.05 by Mann Whitney U test in **i** (n = 6 tumors per group; data represents mean ± s.d.). **(j, k)** Bar graphs show quantification of tumorsphere numbers in control, p63-KD2 and Fzd7-KD tumor MECs (10,000 cells) from Blg-Cre-Brca1$^{f/f}$p53$^{+/-}$ and MMTV-Myc tumors respectively (n = 3 tumors per genotype; data represents mean ± s.d.). P value was computed by Student's t test. *p < 0.05. Size bar, 40 μm in **c.** Uncropped images of blots are shown in Supplementary Fig. 9.

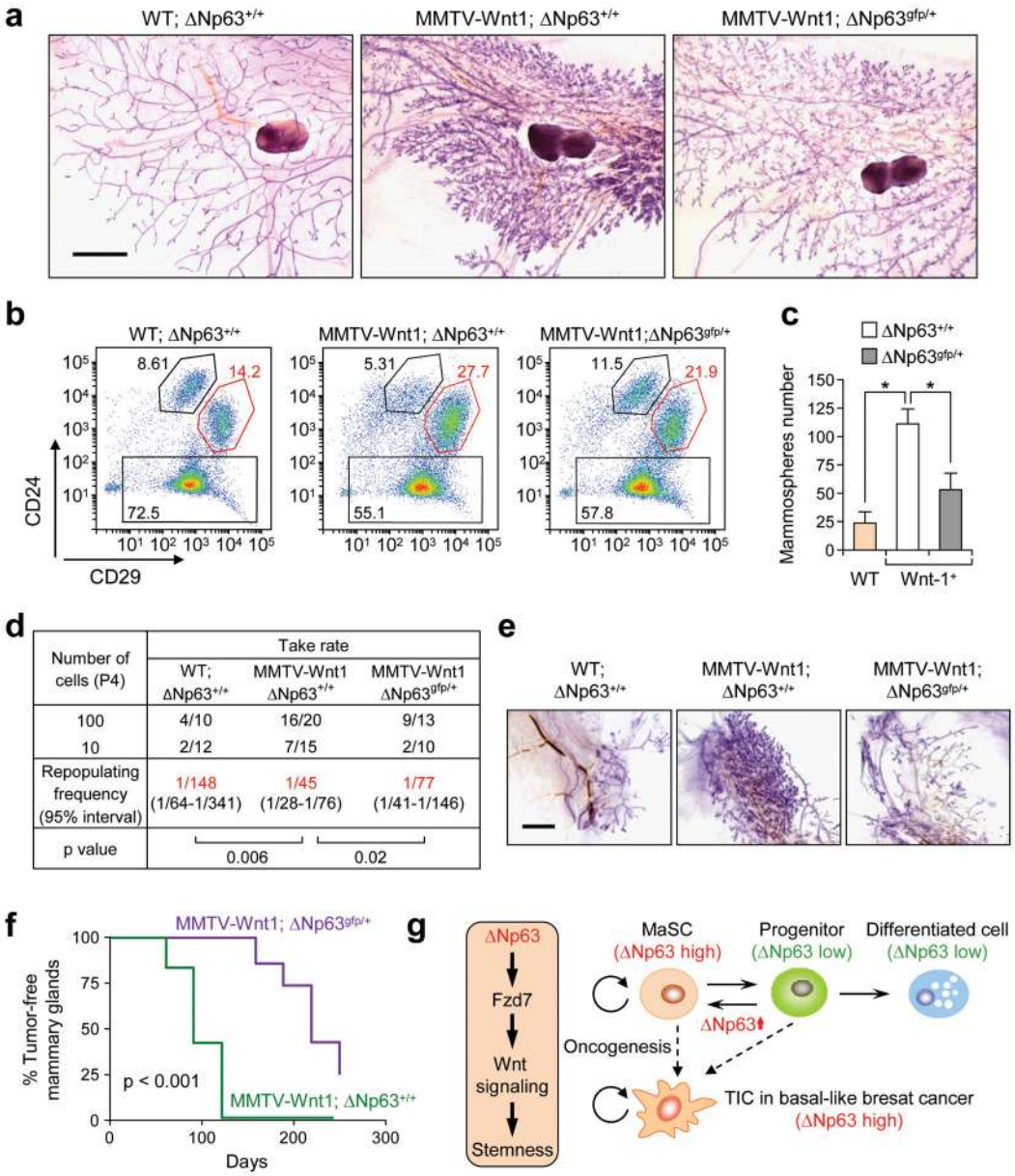

Number of cells (P4)	Take rate		
	WT; ΔNp63+/+	MMTV-Wnt1 ΔNp63+/+	MMTV-Wnt1 ΔNp63gfp/+
100	4/10	16/20	9/13
10	2/12	7/15	2/10
Repopulating frequency (95% interval)	1/148 (1/64-1/341)	1/45 (1/28-1/76)	1/77 (1/41-1/146)
p value		0.006	0.02

Figure 8. Loss of ΔNp63 attenuates Wnt1-driven hyperplasia and tumorigenesis

(a) Representative mammary gland whole mounts from 5- and 8-week-old WT; ΔNp63$^{+/+}$, MMTV-Wnt1; ΔNp63 $^{+/+}$ and MMTV-Wnt1; ΔNp63$^{gfp/+}$ mice. **(b)** Representative FACS profiles of mammary epithelial cells from the indicated. **(c)** Quantification of mammospheres formed by P4 cells (10,000 cells) from 8-week-old mice of indicated genotypes (n = 3 samples, data represents mean ± s.d.).*p < 0.05 by Student's t test. **(d)** Table showing reconstitution efficiency at limiting dilution of P4 cells from mice of the indicated genotypes (n = number of mammary fat pad injections as indicated in the table). P value was obtained by Pearson's Chi-squared test using ELDA software. **(e)** Representative images of outgrowths from **d. (f)** Kaplan-Meier curve analysis of tumor-free mammary glands at the indicated ages (n = 12 mice for MMTV-Wnt1; ΔNp63 $^{+/+}$ and n = 10 mice for

MMTV-Wnt1; ΔNp63 $^{gfp/+}$). Log rank test was used for statistical analysis. **(g)** Schematic model for function of the ΔNp63-Fzd7 axis in mammary cell fate regulation and basal breast cancer initiation. High expression of ΔNp63 in mammary stem cells and TICs maintain their self renewal abilities through activating Fzd7 expression and Wnt signaling. High expression of ΔNp63 can also confer luminal differentiated/progenitor cells with MaSC-like properties. While TICs in basal-like breast cancer may arise from the oncogenic transformation of MaSCs with intrinsic elevated expression of ΔNp63, progenitor cells may also acquire high ΔNp63 expression during their transformation to become TICs. Size bar, 3 mm and 2 mm respectively in **a** and **e**.